International Journal of Microwave and Wireless Technologies

cambridge.org/mrf

Bioinspired planar switched beam network using Butler matrix on a flexible substrate targeting multifaceted millimeter-wave applications

Balaka Biswas[1] and Ayan Karmakar[2]

[1]Department of Electronics and Communication Engineering, Chandigarh University, Mohali, India and [2]Department of MEMS Testing and Application Division, Semi-Conductor Laboratory (SCL), Chandigarh, India

Research Paper

Cite this article: Biswas B, Karmakar A (2024) Bioinspired planar switched beam network using Butler matrix on a flexible substrate targeting multifaceted millimeter-wave applications. *International Journal of Microwave and Wireless Technologies*, 1–11. https://doi.org/10.1017/S1759078724000400

Received: 16 June 2023
Revised: 27 February 2024
Accepted: 14 March 2024

Keywords:
bioinspired antenna; Butler matrix; circuit modeling; crossover; hybrid; LCP; mmW; phase shifter

Corresponding author: Balaka Biswas; Email: balaka.biswas@gmail.com

Abstract

This paper details the design and development of a planar switched beam network using 4 × 4 Butler matrix (BM) over a thin and flexible type biocompatible substrate. Four mils thick liquid crystal polymer (LCP) is used as a substrate here ($\epsilon_r = 2.92$, $\tan\delta = 0.002$). The proposed design is centered at 28 GHz, targeting commercial millimeter-wave applications. Floral-shaped antenna with defective ground structures has been implemented as basic radiating elements. The whole structure is based on microstrip line configuration. The architecture occupies an area of 23.85 × 19.20 mm^2 over the LCP substrate. Individual components of the BM are detailed here, followed by a system analysis of the whole integrated structure. The present work also covers the electrical equivalent circuit modeling of the whole beam-forming network. The fabricated prototype offers better than 18 dB return losses at each input port for the desired frequency band with 6 dBi (max.) peak gain and 500 MHz bandwidth around the center frequency. Port-to-port isolation of better than 15 dB is achieved with this topology. Experimental and simulated results are in good agreement in all aspects. A comparative study is also chalked out to highlight the significance of the current research work with respect to alike earlier reported structures.

Introduction

The last few decades have witnessed the explosive growth of wireless communication. "Antenna" is an indispensable component in the systems used in such wireless communication. Modern day communication needs "smart antenna" in the field of sitcom, navigation, RADAR application, microwave imaging, and even for the 5G network. Switch beam networks find wide application in this gigantic augmentation to realize electronic scanning method. The scanning is accomplished by altering the orientation of the antenna's radiation pattern. The traditionally employed mechanical scanning system suffers due to the wear and tear problem associated with bulky body parts. On the contrary, electronic means of scanning offer multiple technological advantages, viz lightweight, complete removal of wear and tear problems, easy controlling mechanism, etc. Historically, this scanning system was employed in the wireless communication field to mitigate two prime challenges, named "multipath fading" and "inferences" [1]. Continuous scanning applications require "phased array" antenna structures. However, scanning in a single dimension can be achieved by incorporating the concept of switched beam topology. Various phase distributions of the beam-forming network can produce independent beams with different orientations.

Keeping in view of future wireless communication for multi-gigabit services with high data rates, the millimeter-wave (mmW) frequency spectrum is of utmost importance. The mmW spectrum in the 28–38 GHz band [2–8] has applications in the outdoor 5G cellular system; local multipoint distribution services, cellular backhaul, and intra-cell communication systems [9]. Even this particular band of frequency has immense potential in various biomedical applications, such as MRI systems, imaging, etc.

Practically, there are three main categories of Radio frequency (RF) beam-forming networks that have been developed, such as Blass matrix [10], Rotman lens [11], and Butler matrix (BM) [12]. Blass matrix and Rotman lens mainly suffer due to design-oriented challenges. Traditionally, Blass matrix suffers from excessive losses and larger in size [13]. In Rotman lens architecture, beam angle and beamwidth change dynamically with operating frequency, which becomes main disadvantages while a constant beamwidth is demanded [14]. Additionally, efficiency is also restricted due to dummy ports. On the contrary, BM is preferred in terms of design topology, higher efficiency, and minimum RF loss [15]. This topology can produce uniform amplitude distributions. It has some inherent characteristics, such as orthogonal

beam formation, high directivity, very less number of circuit elements, low fabrication cost, etc. Furthermore, it can generate multiple fixed overlapping antenna beams creating wide angular coverage area. Several structures have been reported incorporating circulators [16, 17] and multilayer fabrication strategies [18, 19]. However, these structures invite complexity in terms of fabrication as well as in measurement methods. In comparison to that, the planar version of the same is appreciated for its easier implementation techniques and experimentation. In the modern communication world, while miniaturization plays an important role, multifaceting conformal properties act as an addendum to the planar version of portable devices [20–32].

In the current research work, a planar switched beam network using the BM is presented over a low-loss, thin, flexible substrate named liquid crystal polymer (LCP). It is a biocompatible, radiation-resistant, and high-frequency substrate (even go up to 110 GHz) with very low water absorption capability (<0.04%) [26, 27].

The targeted frequency of operation is chosen as 28 GHz, which falls under the mmW band. Floral-shaped (bioinspired) antenna elements with defective ground structures are employed here. The whole architecture is based upon microstrip geometry, which offers an easy procedure for manufacturing the structure along with ease of testing.

In the subsequent sections, detailed design of BM with electromagnetic wave (EM) simulation results, equivalent circuit modeling, and fabrication of prototypes with measured results have been elaborated.

Elements of beam-forming network

Many pieces of literature are already available on the topic of BM; however, most of the designs focus on the enhancement of the overall bandwidth of the network by implementing multilayer techniques. In this current research work, one of the targets is to make an efficient, low-cost antenna array for biomedical applications that can be easily manufactured. Due to this reason, we have employed a single-layer planar design over a biocompatible and flexible microwave substrate for the BM feed network. Individual building blocks of the beam former are explained in subsections Design of 3-dB directional coupler, wideband crossover, 45° phase shifter, bio inspired antenna and also the building blocks of Butler matrix.

A typical four-beam BM contains four numbers of 3-dB quadrature directional couplers, one 0-dB RF crossover, and two 45° phase shifters. The aim of this network is to feed the neighboring antenna elements with equal amplitude and equally varying phase shifts. Different phase shifts arise while different input ports are exited and that lead the resultant antenna beam to switch in different orientations. Figure 1 depicts such a scheme. Each input or feeding point is responsible for producing different sets of linear phases that are orthogonal in nature. Each individual set is used as an input for the antenna array to form multiple beams in the desired directions.

Considering the linear-phase distribution and exciting the input port, the resultant antenna beam at the output is tilted by the angle given by Equation (1) [1],

$$\theta_p = sin^{-1}\left[\frac{(N+1)-2p}{2N} \times \frac{\lambda}{d}\right] \quad (1)$$

where p varies from 1, 2, ... N; λ = free-space wavelength, d = distance between adjacent antenna elements, $N = 2^n$ (here $n = 2$) no. of radiators.

Design of wideband quadrature 3-dB directional coupler

Traditionally, it is known that a quadrature directional coupler has the ability to provide 90° out-of-phase signals at the output ports with an equal magnitude of power levels [28]. It consists of a primary transmission line, coupled with a secondary transmission line by two-quarter wavelength ($\lambda g/4$) long sections spaced $\lambda g/4$ distance apart (Fig. 2). S-parameter of this four-port network can be written as in Equation (2). The coupler design is finalized for the frequency band of 24–30 GHz. It is based upon the use of Rogers ULTRALAM 3850 laminate (LCP), which has a permittivity of 2.92, a loss tangent of 0.0028, and a thickness of 0.1 mm.

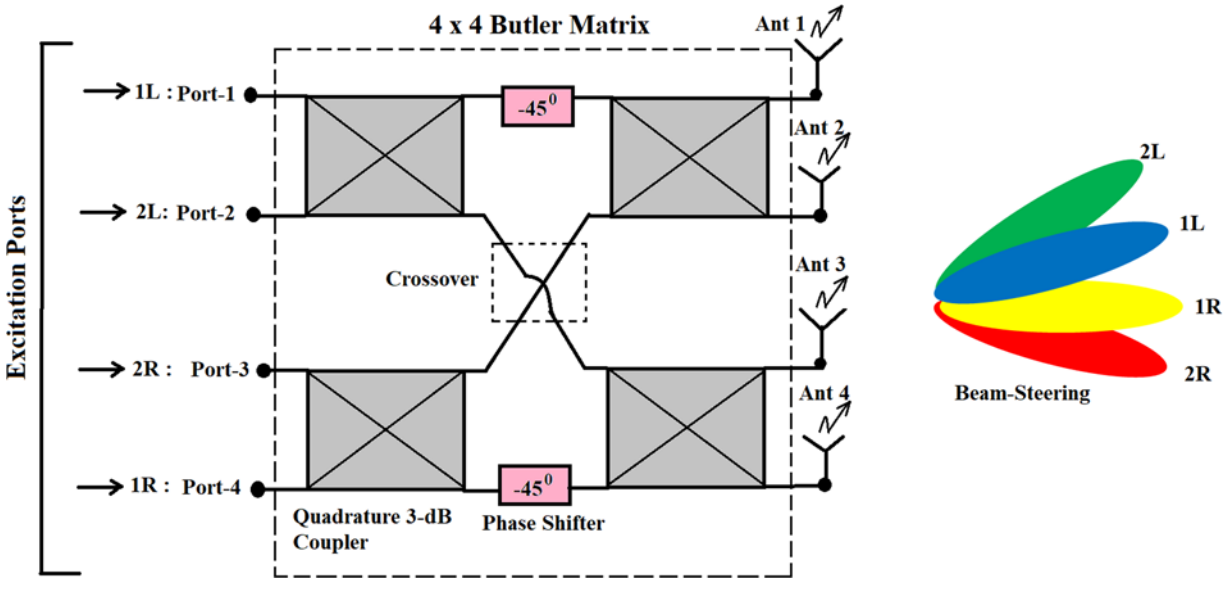

Figure 1. Schematic design of 4 × 4 Butler matrix.

https://doi.org/10.1017/S1759078724000400 Published online by Cambridge University Press

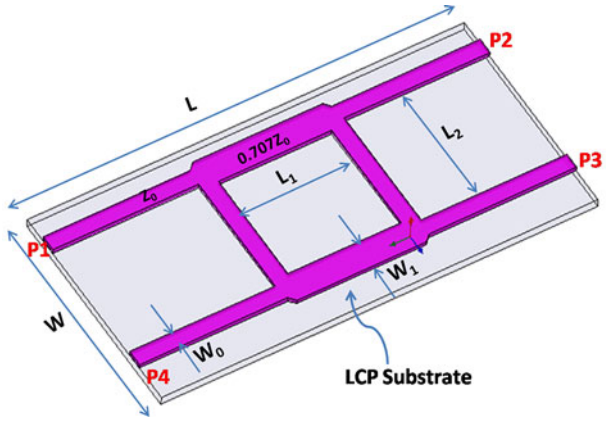

Figure 2. Wideband quadrature coupler design.

Table 1. Optimized dimension of the coupler and crossover designs

Circuit	W (mm)	W_0 (mm)	W_1 (mm)	W_2 (mm)	L (mm)	L_1 (mm)	L_2 (mm)
Coupler	3	0.223	0.384	–	6.005	1.559	1.720
Crossover	3	0.223	0.384	0.632	8.196	1.559	1.559

The coupler is fed by a 50 Ω (Z_0) microstrip line with the geometrical specifications depicted in Table 1 (Fig. 2). The simulated results demonstrate a phase imbalance of less than ±3°, an amplitude imbalance of less than 0.5 dB, and an isolation of better than 15 dB for the entire desired band (Fig. 3)

$$[S] = -\frac{1}{\sqrt{2}}\begin{bmatrix} 0 & j & 1 & 0 \\ j & 0 & 0 & 1 \\ 0 & 1 & j & j \\ 0 & 1 & j & 0 \end{bmatrix} \tag{2}$$

$$S_{21} = jS_{31} \tag{2.a}$$

$$S_{24} = -jS_{34}. \tag{2.b}$$

Design of wideband crossover

Planar wideband crossovers based on Lange couplers have been widely reported in literature [20–27]. However, these designs have constraints due to its fabrication intricacies, as multiple electrical connections are essential in a Lange coupler. A comparatively simpler design is adopted in this current research work by cascading two wideband quadrature directional couplers. It alleviates all the associated fabrication issues. Full-wave analysis of the structure results in optimized dimensions, as depicted in Table 1 (Fig. 4). The proposed structure offers an insertion loss of around 1.5 dB (max.), impedance matching of better than 16 dB, and isolation of better than 14 dB for the entire design frequency band of 24–29 GHz (Fig. 5). S-parameter of an ideal four-port RF crossover network can be expressed in terms of Equations (3–9)

$$[S] = \begin{bmatrix} 0 & 0 & 1 & 0 \\ 0 & 0 & 0 & 1 \\ 1 & 0 & 0 & 0 \\ 0 & 1 & 0 & 0 \end{bmatrix}. \tag{3}$$

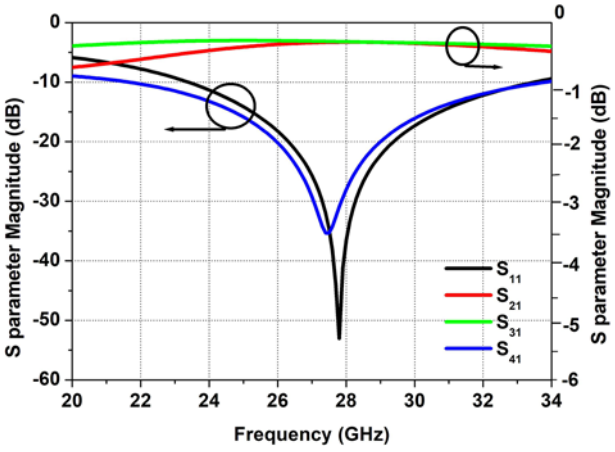

Figure 3. S-parameter of the coupler.

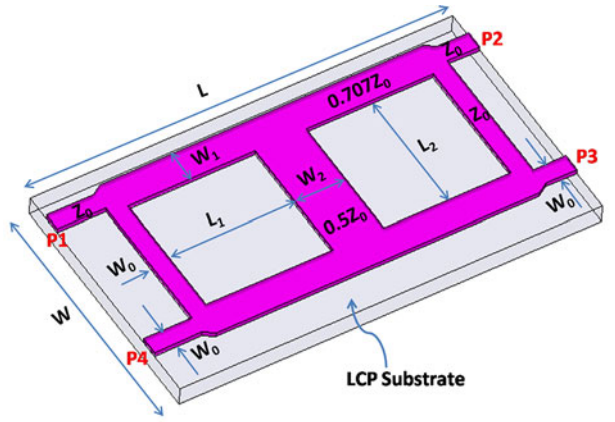

Figure 4. Wideband crossover design.

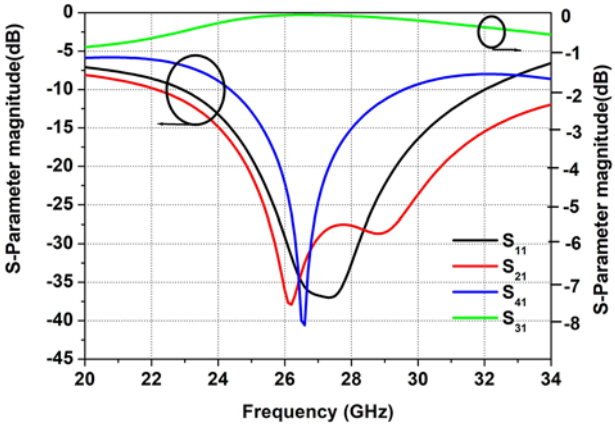

Figure 5. S-parameter of the crossover.

An ideal crossover is governed by the following S-parameters:

$$S_{11} = S_{21} = S_{41} = 0; \quad |S_{31}| = 1. \tag{4}$$

Equation (4) depicts that, if one injects some power into port 1, none of it goes to port 2. All the power goes cross coupled into port 3, whereas port 4 is an isolated port. Layout of phase shifter is shown in Fig. 6. Owing to the presence of fully symmetry

https://doi.org/10.1017/S1759078724000400 Published online by Cambridge University Press

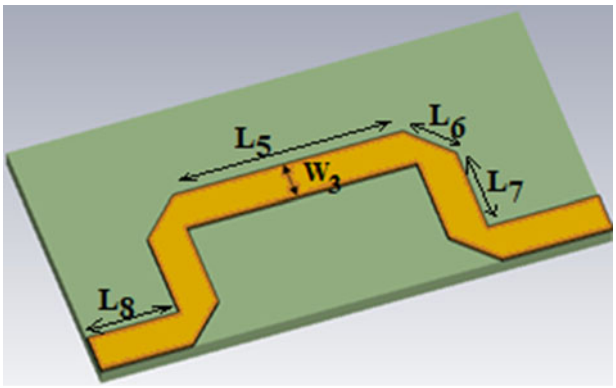

Figure 6. Layout of the phase shifter.

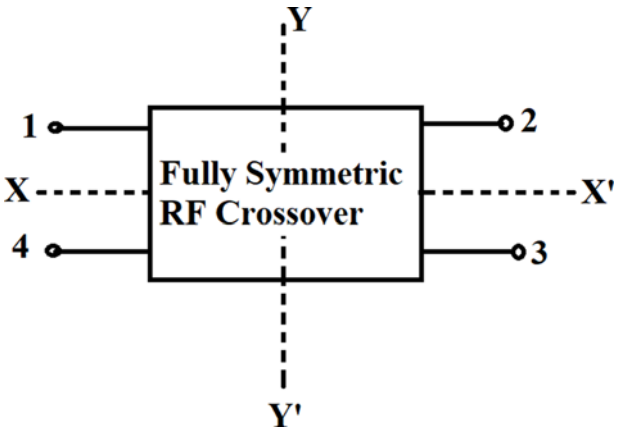

Figure 7. Black-box diagram of a fully symmetric RF crossover core. XX′ and YY′ are the two axes of symmetry.

(even-odd mode) analysis can be invoked in Fig. 7, which results into four eigen admittances

$$Y_{ij}\left[i=\{o,e\},\ j=\{o,e\}\right]. \tag{5}$$

These admittances are related to S-parameters as follows [28]

$$S_{11}=\frac{\Gamma_{ee}+\Gamma_{eo}+\Gamma_{oe}+\Gamma_{oo}}{4} \tag{6}$$

$$S_{21}=\frac{\Gamma_{ee}-\Gamma_{eo}+\Gamma_{oe}-\Gamma_{oo}}{4} \tag{7}$$

$$S_{31}=\frac{\Gamma_{ee}-\Gamma_{eo}-\Gamma_{oe}+\Gamma_{oo}}{4} \tag{8}$$

$$S_{41}=\frac{\Gamma_{ee}+\Gamma_{eo}-\Gamma_{oe}-\Gamma_{oo}}{4} \tag{9}$$

where $\Gamma_{ij}=\frac{1-Z_0Y_{ij}}{1+Z_0Y_{ij}}$, $Z_0=$ port termination impedance.

Design of 45° phase shifter

For the present research work, the BM requires two numbers of 45° phase shifters. It is realized by choosing the suitable length of the

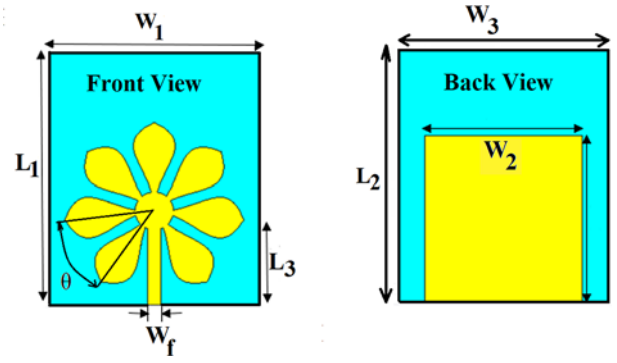

Figure 8. Proposed bioinspired antenna.

50 Ω transmission line as governed by Equation (10) [29]

$$\theta=\beta.\ell \tag{10}$$

where θ is the phase shift required (here it is 45°); β is phase constant ($=2\pi/\lambda_g$); λ_g is guided wavelength, and ℓ is the physical length of the transmission line. For our case, ℓ is coming around 0.76 mm. Figure 6 demonstrates the structure of the phase shifter with optimized design dimensions ($W_3=0.223$, $L_5=0.56$, $L_6=0.2$, $L_7=0.1$, and $L_8=0.1$ mm). S-parameter of the phase shifter can be expressed as Equation (11)

$$[S]=\begin{bmatrix}0 & 1+j\\ 1-j & 0\end{bmatrix}. \tag{11}$$

Design of bioinspired antenna

A printed version of the monopole antenna with bioinspired geometry is proposed for the beam-forming network (Fig. 8). The said antenna looks like a flower with seven petals. Miniaturization and enhancement of directive gain for the individual antenna elements are achieved by this biomimicry method [30–34].The bioinspired geometry of Jasmine-shaped flower increases the perimeter of the antenna compared to a classical patch antenna (microstrip) and consequently the frequency behavior. The electric length of the radiator increases, which helps to attain high gain. From a mathematical point of view, this flower-shaped radiator is a class of fractal, which refers to a set in Euclidean space with specific properties, such as self-similarity or self-affinity. In this fractal shape, polar transformations give rise to a wide class of shapes. This polar transformation can be defined through a vector function

$$\bar{\nu}(t)=\left[\left(x(t),y(t)\right)\right],\ t\geq 0; \tag{12}$$

that is, for each real value, t is associated with a vector in $\mathcal{R}^2$, Equation (13)

$$\bar{\nu}(t):I\rightarrow\mathcal{R}^n \tag{13}$$

$$t\rightarrow\bar{\nu}(t)$$

The proposed radiator occupies an area of 5.08 × 4.14 mm^2 over the LCP substrate [35].

The shape of the petals is governed by the analytic curve following Equation (14). Each of the petals consists of two same types of Chebyshev tapering. It is formed by choosing an independent

https://doi.org/10.1017/S1759078724000400 Published online by Cambridge University Press

Table 2. Optimized dimension of the floral-shaped antenna

L_1 (mm)	L_2 (mm)	L_3 (mm)	W_1 (mm)	W_2 (mm)	W_f (mm)	Θ (degree)
5.08	3.36	1.54	4.14	3.12	0.247	48

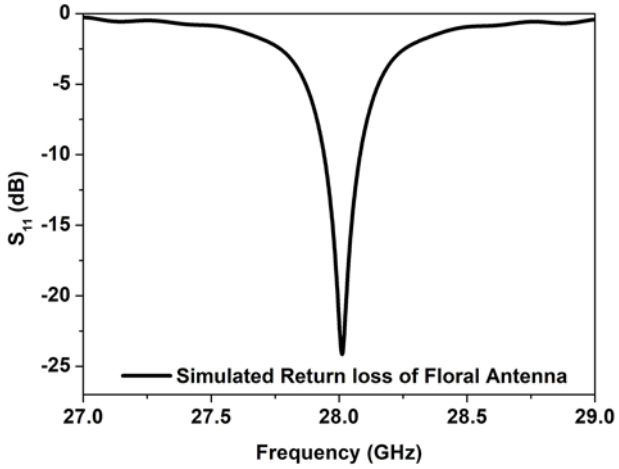

Figure 9. Reflection coefficient for the antenna.

variable, "L". Then, each petal is rotated by an angle of "θ"

$$y = N \times (t/L)^5 - (t/L)^2. \tag{14}$$

Here, t is the variable, with respect to which the equation varies; it varies between 0 and L. The variable L is responsible for length of the petal, whereas N determines its width,

$$\text{where, } \theta = \tan\left(\frac{\frac{W_2}{2} - \frac{W_f}{2}}{L_3}\right) \tag{15}$$

Parametric EM simulation refers to the optimized dimension of the antenna as summarized in Table 2. The reflection parameter reveals that the floral-shaped antenna is well matched (>10 dB) for a narrow-band centering at 28 GHz (Fig. 9) with 5.6 dBi directive gain. For the present work, the radiating element faces a loading effect of the BM at the input point. Hence, careful matching of the impedance profile for the desired frequency band (28 ± 0.25 GHz) is mandatory.

Integration of building blocks of BM

Individual building blocks, explained in the previous subsections, are integrated systematically to form the feed network of the beam former (Fig. 10). It acts as a passive microwave network with eight numbers of I/O ports, which offers better than 8 dB return losses for the desired frequency band of the antenna (27.75–28.25 GHz), as shown in Fig. 11 for all different excitation ports. Ports 1–4 are excitation ports, and ports 5–8 are designated as output ports, which are used further to excite the radiating patches. Patches are placed equidistantly (0.65 λg) by adjusting a suitable meandering technique in 50 Ω lines, emanating from all output ports of the feed network (Fig. 12). Table 3 summarizes the overall dimension of the beam-forming network.

The beam-steering property of the whole Butler matrix was computed by feeding the input signals from different input ports.

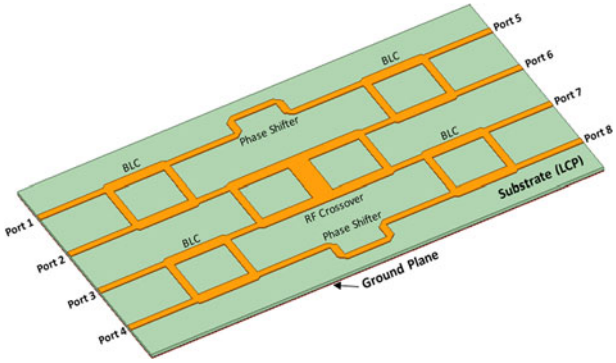

Figure 10. Feed network of beam-forming smart antenna.

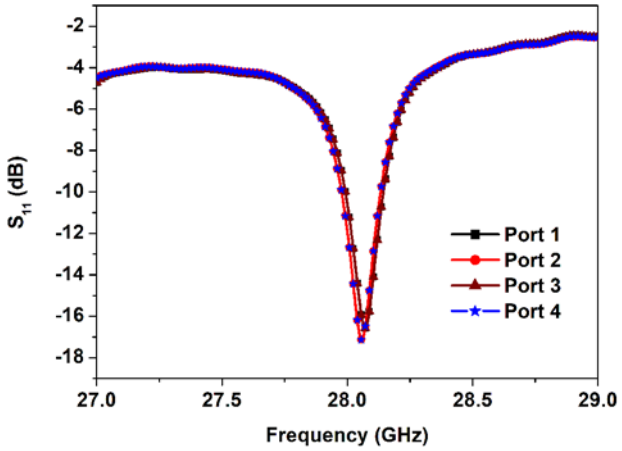

Figure 11. S_{11}-parameter for all input ports.

Figure 13 demonstrates the orientation-dependent radiation characteristics in both the E and H planes. Here, characteristics have been shown only for two ports, as the rest of the two ports will be just symmetric ones instead of 180° phase shifts. It is clearly visible that there is a signature of beam-steering for different port excitations. It infers the exhibition of smart antenna engineering, implementing the electronically scanning array technique.

Equivalent circuit modeling of Butler network

In the proposed topology, the antenna array, along with the beam-forming network, acts as a transmitter. In this transmission mode, the antenna itself appears as a load on the generator [36, 37–39]. An equivalent circuit representation of the transmitter (Tx) array antenna with beam-former is shown in Fig. 14.

where Z_G = equivalent impedance of generator $[Z_G = (R_G + jX_G)]$

$Z_B = R_B + jX_B$ = equivalent impedance of BM

I_{in} = current at the antenna's input terminal

$$\left[I_{in} = \frac{V}{(Z_G + Z_B + Z_A)}\right] \tag{16}$$

Z_A = equivalent antenna's impedance at terminals a–b

$$= R_A + jX_A = (R_L + R_{rad}) + jX_A \tag{17}$$

V_{th} = induced voltage at antenna while incident wave impinges upon it, this is analogous.

https://doi.org/10.1017/S1759078724000400 Published online by Cambridge University Press

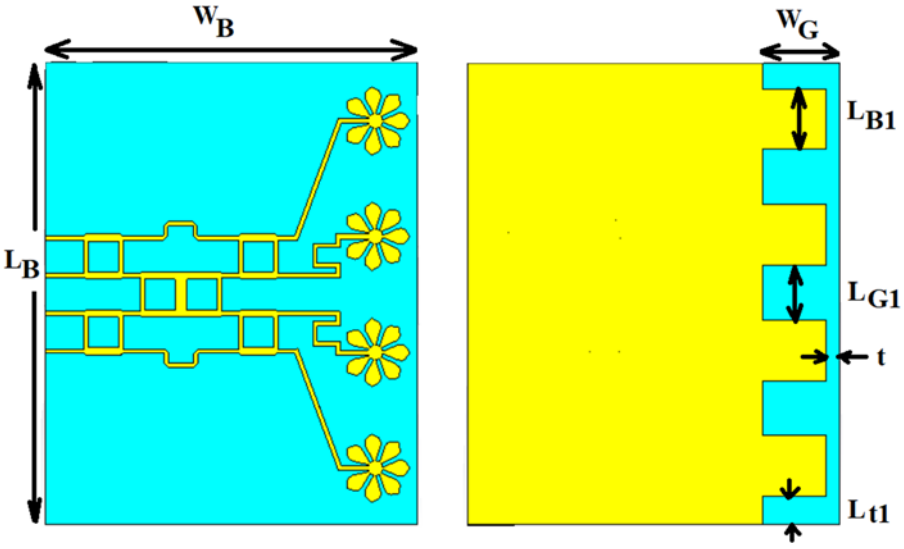

Figure 12. Complete architecture of the proposed Butler matrix (left – front view; right – rear view).

Table 3. Optimized dimension of the Butler matrix

L_B (mm)	W_B (mm)	W_G (mm)	t (mm)	L_{B1} (mm)	L_{G1} (mm)	L_{t1} (mm)
23.85	19.2	5.08	1.72	3.12	3.12	1

R_A = antenna resistance at terminals a–b
R_L = loss resistance of antenna
R_{rad} = radiation resistance of antenna
R_G = resistance of generator impedance
X_G = reactance of generator impedance
X_A = antenna reactance at terminals "a–b"
X_B = reactance of BM's impedance
R_B = resistance of BM's impedance.

The total power (P_{Tot}) produced by the generator is the summation of power delivered to the antenna terminals (P_T) and the power lost (P_G) in the generator's internal resistance R_G.

Thus,

$$P_{Tot} = P_T + P_G. \tag{18}$$

Again, a portion of P_T is radiated away (P_{rad}), and the rest amount is dissipated as Ohmic losses, P_{Ohm}.

Thus,

$$P_T = P_{rad} + P_{Ohm}. \tag{19}$$

Equation (3) can be expressed as,

$$P_T = \frac{1}{2}|I_{in}|^2 R_A = \frac{1}{2}|I_{in}|^2 [R_{rad} + R_L]. \tag{20}$$

Power delivered to the antenna (array) for radiation,

$$P_{rad} = \frac{1}{2}[I_{in}]^2 R_{rad}$$

$$= \frac{1}{2}[V_g]^2 \left[\frac{R_{rad}}{(R_{rad} + R_L + R_G + R_B)^2 + (X_A + X_G + X_B)^2}\right]. \tag{21}$$

Overall antenna efficiency is given by [25]

$$e_0 = e_r e_c e_d \tag{22}$$

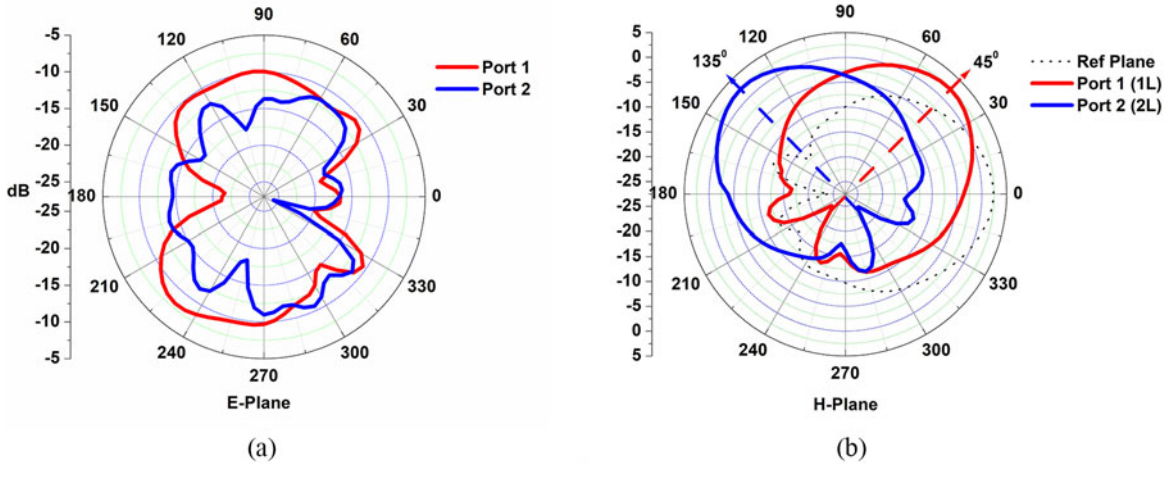

Figure 13. Far-field radiation pattern of the Butler matrix with different port excitations.

https://doi.org/10.1017/S1759078724000400 Published online by Cambridge University Press

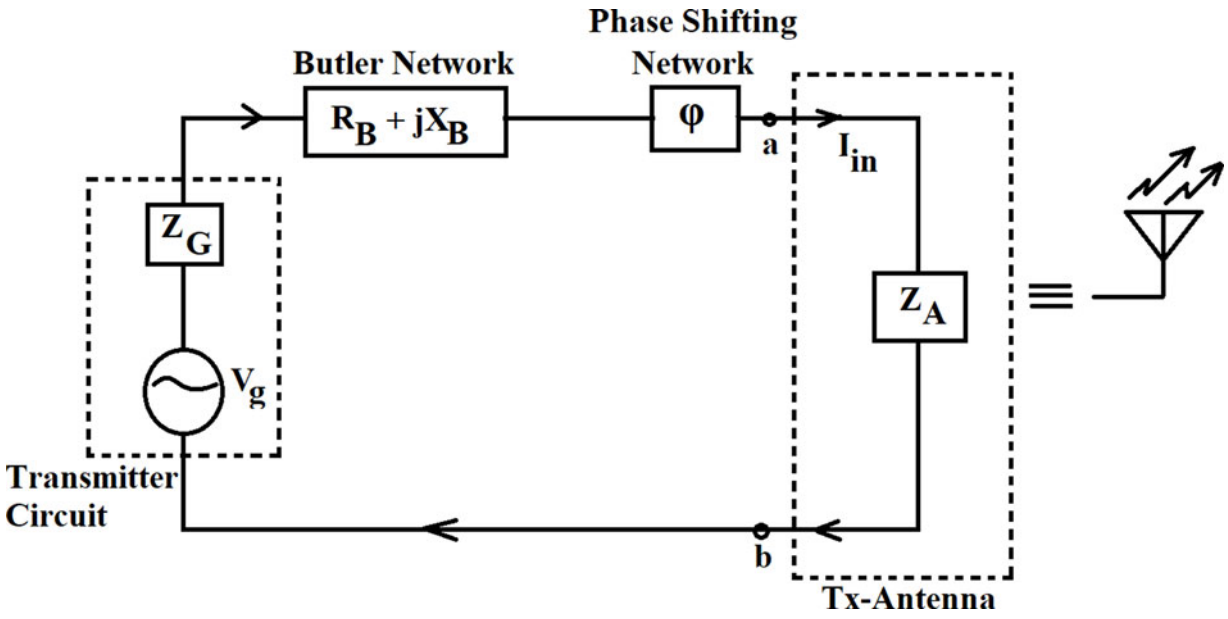

Figure 14. Circuit modelling of Butler network.

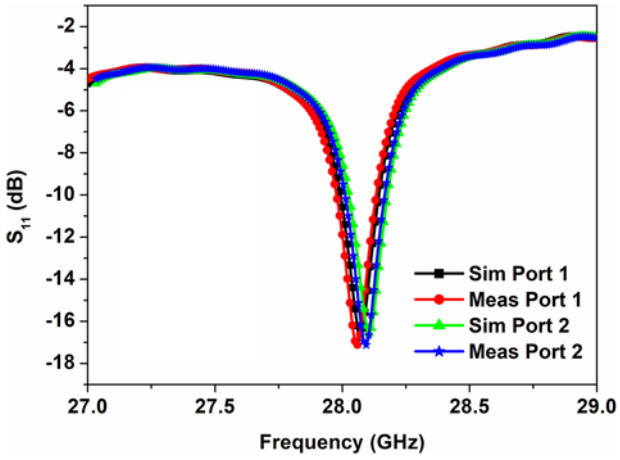

Figure 15. Simulated and measured results.

where e_0 = total efficiency, e_r = mismatch efficiency,
$e_r = \left(1 - |\tau|^2\right)$, e_c = conduction efficiency, e_d = dielectric efficiency, τ = Voltage standing wave ratio (VSWR) at antenna input terminal.

$$\tau = \frac{Z_{in} - Z_0}{Z_{in} + Z_0} \tag{23}$$

where Z_{in} = input impedance of the antenna
Z_0 = characteristic impedance of Tx line.

Usually, e_c and e_d are very difficult to evaluate separately [35]. Hence, traditionally e_0 is written as

$$e_0 = e_{cd}\left(1 - |\tau|^2\right). \tag{24}$$

This radiation efficiency can be obtained through Wheeler's cap method [40] and directivity/gain measurement. Equivalent circuit of antenna has a very little to do with it. However, e_0 can be expressed as follows:

$$e_0 = \frac{R_{rad}}{(R_{rad} + R_B + R_L)}. \tag{25}$$

Fabrication and measurement

The proposed BM has been fabricated on a thin (100 ± 10 μm), flexible, and biocompatible LCP substrate. Standard photolithography and wet-etching chemistry are adopted to realize the geometry. It is very clear that all four input ports are placed in close proximity, which restricts the assembly of standard RF connectors to them for signal launching. Hence, it evokes some measurement-related practical issues. It is solved here with the use of air coplanar probe (ACP)-type RF coplanar probes (ground-signal-ground: GSG) [38] of 150 μm pitch size. The in-house made coplanar waveguide in microstrip patch (CPW-MS) [39–46] transition makes a suitable alternative for RF measurement and launching of signals from probes to microstrip feed lines of Butler networks. De-embedding techniques were adopted to achieve the intended response of the device under test (DUT). Figure 15 depicts the return loss profiles for all of the input ports on the fabricated prototype. Figure 16 shows the front and rear view of fabricated prototype on flexible substrate along with the transition structure. The flexibility of the substrate is also observed from the same. Further, in the compact antenna test facility, the radiation characteristics of the prototype antenna are evaluated. It shows a maximum gain of around 5.8 dBi. The far-field radiation pattern is exhibited in Figs. 17 and 18 for different input ports. The performance metrics of the antenna infer that it is a high-gain and narrow-band candidate, mostly suitable for detecting the tumor cell/malignant tissue at a precise operating frequency in the mmW band. Even so, it can be used for radiotherapy or mmW hyperthermia applications. A comparison table (Table 3) is included here to discuss various performance metrics of the proposed network with respect to recently reported structures. It can be inferred that our work occupies minimum layout area over thin substrate for the same 4 × 4 BM configuration to

https://doi.org/10.1017/S1759078724000400 Published online by Cambridge University Press

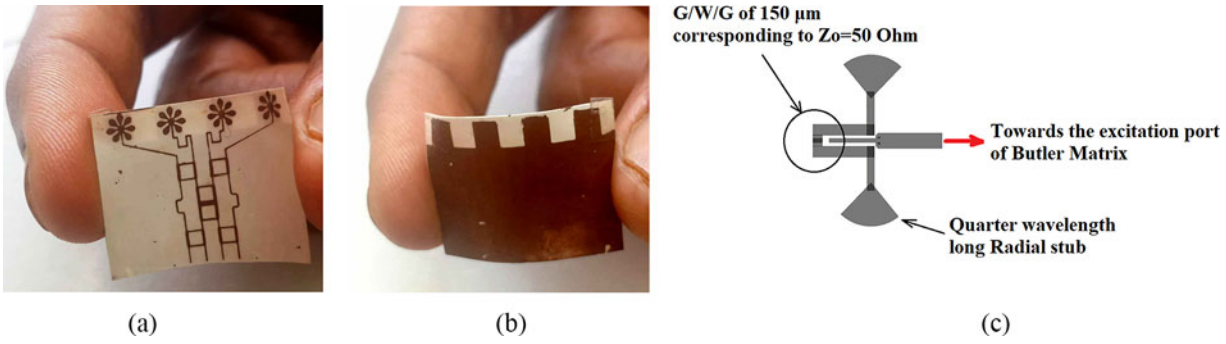

Figure 16. Fabricated prototype: (a) front view, (b) rear view, and (c) CPW-MS transition structure used at the time of measurement.

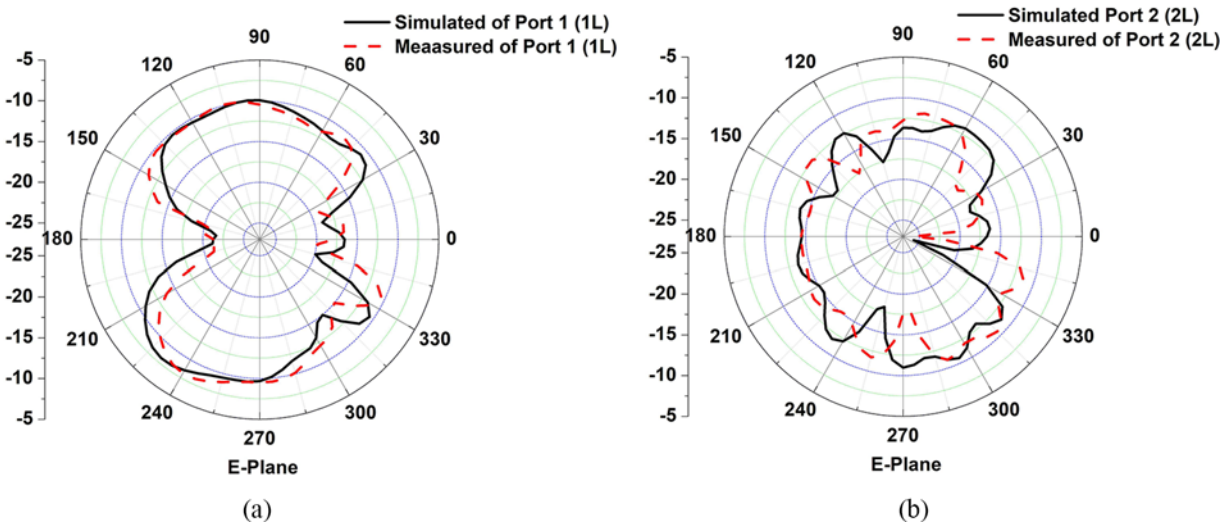

Figure 17. Simulated and measured far-field pattern in *E*-plane of the Butler matrix at 28 GHz.

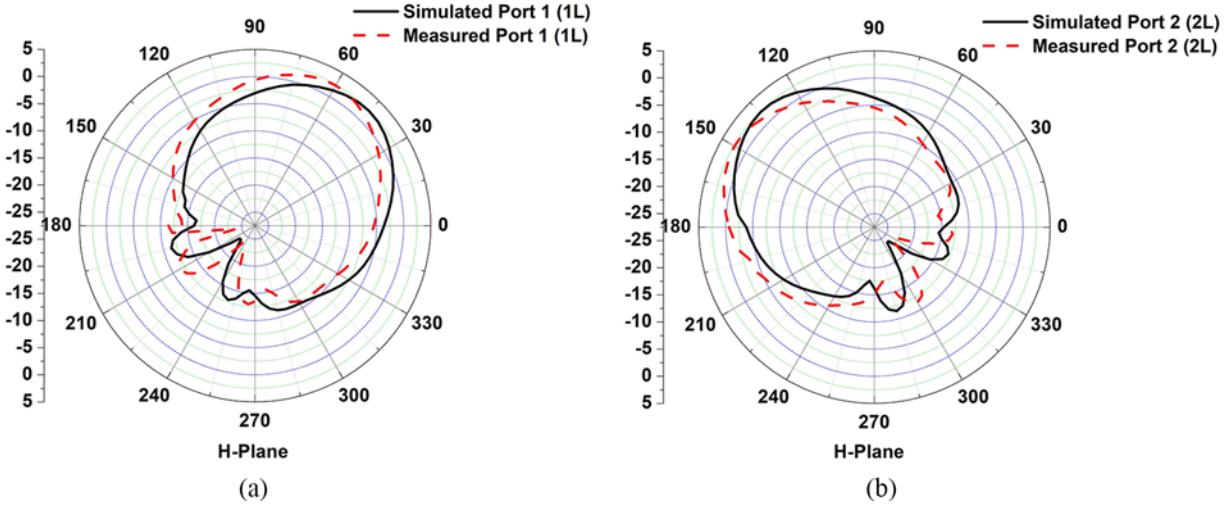

Figure 18. Simulated and measured far-field pattern in *H*-plane of the Butler matrix at 28 GHz.

provide appreciable gain (>5 dBi) with satisfactory port to port isolation than that of (>15 dB) earlier reported results.

A comparison table is provided in (Table 4) that compares the proposed work with recently reported structure. The gain characteristic of the bioinspired antenna is shown in the Fig. 19. It has been shown that maximum gain of the antenna is 5.8–6 at the desired frequency band.

Conclusion

This work reports the design and development of a novel configuration for a planar switched beam network targeting multifaceted mmW applications. The novelty of the current research work comes from the implementation of the bioinspired antenna in the BM configuration along with the usage of flexible and

https://doi.org/10.1017/S1759078724000400 Published online by Cambridge University Press

Table 4. Comparison of performance metrics of proposed network amongst recently reported structures

Ref.	Year	Center frequency (f_0) (GHz)	Bandwidth@f_0	Size (mm^2)	Dimension of Butler matrix	Substrate	Antenna gain (dBi)	Input port-to-port isolation (dB)
[2]	2021	28	78.5%	37 × 50	4 × 4	The Taconic RF-30	5.8–6.7	–
[3]	2017	38	26.3%	64.4 × 60	4 × 8	Rogers 5880	19.8	–
[4]	2021	30	166.66%	–	4 × 4	RO-3003™	11.7	>15
[5]	2019	28	10.71%	36.2 × 44.3	4 × 4	Two-layer hybrid stackup	10	–
[22]	2018	30	30%	60 × 50	4 × 4	RO-3003™	–	–
[24]	2019	30	180%	120 × 70	8 × 8	Rogers ULTRALAM 3850	9–12	>14
This work	2023	28	18%	23.85 × 19.2	4 × 4	Biocompatible LCP	5–6	>15

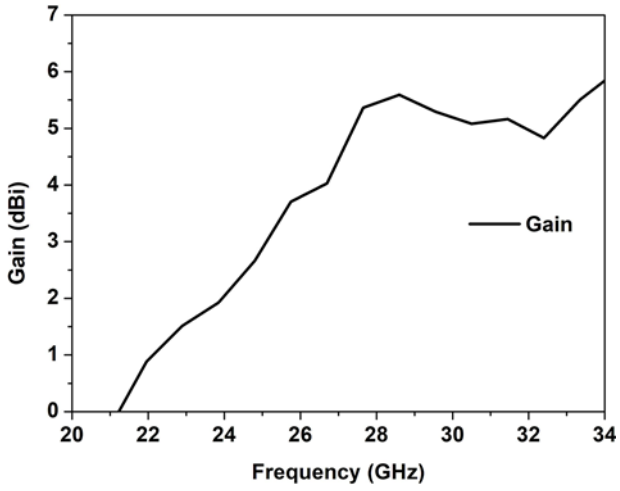

Figure 19. Gain of the bioinspired antenna.

biocompatible LCP substrate. Other reported works [2–5, 22, 24] in this context achieve higher gain and bandwidth, at the cost of a larger layout area. However, the current R&D work exhibits its superiority in all intended performance metrics with its reduced dimension by incorporating the said novelties into the architecture. The proposed design offers a maximum gain of around 5 dBi with 500 MHz bandwidth. Further, it can be enhanced by enlarging the dimension of the BM but at the cost of increased footprint area. The high gain feature with a narrow-band profile makes the current antenna suitable for detecting tumor cells and hyperthermia treatments. Finally, the substrate makes the proposed antenna as a conformal candidate for arbitrary 3D shapes. As per the author's knowledge to date, such a miniaturized antenna based upon planar configuration never has been reported with all state-of-the-art performance metrics for biomedical applications with the flexible substrate.

Acknowledgements. Authors are very much thankful to Mr. Bobby of IISER, Mohali for extending hand of cooperation during the fabrication work.

Competing interests. In accordance with *International Journal of Microwave and Wireless Technologies* policy and our ethical obligations as researchers, we wish to declare that there is no potential conflict of interest was reported by the authors.

References

1. **Robert JM** (2005) *Phased Array Antenna Handbook*. Boston: Artech House.
2. **Lee S, Lee Y and Shin H** (2021) A 28-GHz switched-beam antenna with integrated Butler matrix and switch for 5G applications. *Sensors* **21**, 5128.
3. **Cao Y, Chin KS, Che W, Yang W and Li ES** (2017) A compact 38 GHz multibeam antenna array with multifolded Butler matrix for 5G applications. *IEEE Antennas and Wireless Propagation Letters* **16**, 2996–2999.
4. **Ashraf N, Sebak AR and Kishk AA** (2021) PMC packaged single-substrate 4 × 4 Butler matrix and double-ridge gap waveguide horn antenna array for multibeam applications. *IEEE Transactions on Microwave Theory & Techniques* **69**(1), 248–261.
5. **Kim S, Yoon S, Lee Y and Shin H** (2019) A miniaturized Butler matrix based switched beamforming antenna system in a two-layer hybrid stackup substrate for 5G applications. *Electronics* **8**, 1232.
6. **Lian JW, Ban YL, Xiao C and Yu Z-F** (2018) Compact substrate-integrated 4 × 8 Butler matrix with sidelobe suppression for millimeter-wave multibeam application. *IEEE Antennas and Wireless Propagation Letters* **17**, 928–932.
7. **Chen CJ and Chu TH** (2010) Design of a 60-GHz substrate integrated waveguide Butler matrix—A systematic approach. *IEEE Transactions on Microwave Theory & Techniques* **58**(7), 1724–1733.
8. **Djerafi T and Wu K** (2012) A low-cost wideband 77-GHz planar Butler matrix in SIW technology. *IEEE Transactions on Antennas and Propagation* **60**(10), 4949–4954.
9. **Kutty S and Sen D** (2016) Beamforming for millimeter wave communications: An inclusive survey. *IEEE Communications Surveys and Tutorials* **18**(2), 949–973.
10. **Mosca S, Bilotti F, Toscano A and Vegni L** (2002) A novel design method for Blass matrix beam-forming networks. *IEEE Transactions on Antennas and Propagation* **50**(2), 225–232.
11. **Huang GC and Iskander MF** (2020) Comparative study of wideband Butler matrix and Rotman lens beamforming network for millimeterwave applications at Ka band. In *IEEE International Symposium on Antennas and Propagation and North American Radio Science Meeting*, Montreal, QC, Canada, 1587–1588.
12. **Paschaloudis K, Lialios D, Zekios C, Kyriacou G, Georgakopoulos S and Ntetsikas N** (2020) Design of true time delay millimeter wave beamformers for 5G multibeam phased arrays. *Electronics* **9**, 1–29.
13. **Blass J** (1966) Multidirectional antenna—A new approach to stacked beams. In *Proceedings of the 1958 IRE International Convention Record*, 48–50.

https://doi.org/10.1017/S1759078724000400 Published online by Cambridge University Press

14. **Nolen J** (1965) Synthesis of multiple beam networks for arbitrary illuminations. Radio Division, Bendix Corporation.
15. **Fakoukakis F, Kaifas T, Vafiadis E and Kyriacou G** (2015) Design and implementation of Butler matrix-based beam-forming networks for low sidelobe level electronically scanned arrays. *International Journal of Microwave and Wireless Technologies* **7**(1), 69–79.
16. **Chou HT, Chang CH and Chen YS** (2018) Multibeam microstrip patch antennas excited by parallel-plate beam-forming network with shaped reflecting boundary and optimized slot feeding transition structures. *Radio Science* **43**(11), 1426–1437.
17. **Shelton JP and Hsiao JK** (1979) Reflective Butler matrices. *IEEE Transactions on Antennas and Propagation* **30**, 651–659.
18. **Gatti RV and Riccardo Rossi R** (2016) Single-ridge waveguide T-junctions for compact multilayer beam forming networks. *International Journal of RF and Microwave Computer-Aided Engineering* **27**(1), 1–6.
19. **Wincza K and Sachse K** (2010) Broadband 4×4 Butler matrix in microstrip multilayer technology designed with the use of three-section directional couplers and phase-correction networks. In *IEEE 18th International Conference on Microwave RADAR and Wireless Communications*, 1–4.
20. **Nusenu S and Asare E** (2020) Butler matrix frequency diverse retrodirective array beamforming: An energy-efficient technique for mmWave networks. *Wireless Communications and Mobile Computing* **2020**, 1–12.
21. **Zulkifli FY, Chasanah N and Rahardjo ET** (2015) Design of Butler matrix integrated with antenna array for beam forming. In *International Symposium on Antennas and Propagation (ISAP)*, 1–4.
22. **Ashraf N, Kishk AA and Sebak AR** (2018) AMC packaged - Butler matrix for millimeter wave beamforming. In *2018 IEEE International Symposium on Antennas and Propagation & USNC/URSI National Radio Science Meeting*, 417–418.
23. **Yazdanbakhsh P and Solbach K** (2011) Microstrip Butler matrix design and realization for 7 T MRI. *Magnetic Resonance in Medicine* **66**, 270–280.
24. **Klionovski K, Sharawi MS and Shamim A** (2019) A dual-polarization-switched beam patch antenna array for millimeter-wave applications. *IEEE Transactions on Antennas and Propagation* **67**(5), 3510–3515.
25. **Khadaroo A, Rahim MKA, Khawaja BA and Iqbal MN** (2020) Compact metamaterial based 4 × 4 Butler matrix with improved bandwidth for 5G applications. *IEEE Access* **8**, 13573–13583.
26. **Vyas R, Rida A, Bhattacharya S and Tentzeris MM** (2007) Liquid Crystal Polymer (LCP): The ultimate solution for low-cost RF flexible electronics and antennas. In *IEEE Antennas and Propagation Society International Symposium*, 1729–1732.
27. **Palazzari V, Thompson D, Papageorgiou N, Pinel S, Lee JH, Sarkar S, Pratap R, DeJean G, Bairavasubramanian R, Li R-L, Tentzeris M, Laskar J, Papapolymerou J and Roselli L** (2004) Multi-band RF and mm-wave design solutions for integrated RF functions in liquid crystal polymer system-on-package technology. In *Proceedings of the 2004 IEEE-ECTC Symposium*, 1658–1663.
28. **Maktoomi MA, Makhtoomi MH, Zafar ZN, Helaoni M and Ghannounchi FM** (2009) Simplified analysis of symmetrical RF cross overs extended with arbitrary complex passive two-port networks. *PIER Letters* **85**, 1–8.
29. **Serres A, Serres G, Silva Junior P, Freire R, Cruz J, Albuquerque T, Oliveira M and Silva P** (2017) Bio-inspired microstrip antenna. **10** IntechOpen.
30. **Behdad N, Mudar A, Joumayly A and Meng L** (2011) Biologically inspired electrically small antenna arrays with enhanced directional sensitivity. *IEEE Antennas and Wireless Propagation Letters* **10**, 361–364.
31. **Ebnabbasi K** (2013) A bio-inspired printed-antenna transmission-range detection system. *IEEE Antennas and Propagation Magazine* **55**(3), 193–200.
32. **Ponnapalli VS, Sowjanya, Sudutha R, Abhishek N and Pranitha KS** (2021) Design of bio inspired maple leaf microstrip patch antenna array with different substrates for wireless applications. In *International Conference on Recent Trends on Electronics, Information, Communication & Technology (RTEICT)*, 809–812.
33. **Raviteja GV and Siva Rama Praveen K** (2021) Bio-inspired Korean striped maple leaf (Acer Tegmentosum) microstrip monopole design targeting UWB applications. In *International Conference on Advances in Electrical, Computing, Communication and Sustainable Technologies (ICAECT)*, 1–7.
34. **Biswas B, Ghatak R and Poddar DR** (2017) A fern fractal leaf inspired wideband antipodal Vivaldi antenna for microwave imaging system. *IEEE Transactions on Antennas and Propagation* **65**(11), 6126–6129.
35. **Biswas B, Karmakar A and Adhikar V** (2021) Liquid crystal polymer: Potential bio compatible substrate for antenna application. *Microwave Review* **27**(1), 17–22.
36. **Ponnapalli VAS, Sowjanya, Sudutha R, Abhishek N and Pranitha KS** (2021) Design of Bio Inspired Maple Leaf Microstrip Patch Antenna Array with Different Substrates for Wireless Applications. In *2021 International Conference on Recent Trends on Electronics*, Information, Communication & Technology (RTEICT), Bangalore, India, 809–812.
37. **Biswas B and Karmakar A** (2021) Electrical equivalent circuit modeling of various fractal inspired UWB antennas. *Frequent Journal of RF-Engineering and Telecommunications* **75**(3-4), 109–116.
38. **Orfanidis JS** (2013) Electromagnetic waves and antennas. Rutgers University Press. https://www.ece.rutgers.edu/∼orfanidi/ewa (accessed 1 August 2016).
39. **Balanis CA** (2016) *Antenna Theory: Analysis and Design*, 4th edn. Hoboken, NJ: John Wiley and Sons, Inc.
40. **Wheeler HA** (1959) The radian sphere around a small antenna. *Proceedings of the IRE* **47**, 1325–1331.
41. **Biswas B and Karmakar A** (2022) Customary of CPW configuration's in silicon RF technology targeting monolithic integration for GHz to THz frequency band. *Materials Today: Proceedings* **71**, 220–226.
42. **Karmakar A, Biswas B and Gayen S** (2022) Measurement challenges for On-wafer characterization of RF devices and its remedial solutions targeting multifaceted wireless communication in modern era. In *IEEE MTT-S & APP-S International Microwaves, Antennas and Propagation Conference (MAPCON-2022), 12th–15th*.
43. **Lee S, Lee Y and Shin H** (2021) A 28-GHz switched-beam antenna with integrated butler matrix and switch for 5G applications. *Sensors* **21**, 5128.
44. **Roy B, Karmakar A and Chakraborty U** (2022) Planar switched beam network using Butlar matrix on a single layer substrate for modern wireless communications. *Radio Science* **57**, e2021RS007348.
45. **Biswas B and Karmakar A** (2023) Printed antennas for future generation wireless communication and healthcare, CRC Press Taylor & Francis Group an international publisher of progressive academic research. https://www.routledge.com/Printed-Antennas-for-Future-Generation-Wireless-Communication-and-Healthcare/Biswas-Karmakar/p/book/9781032393018 (accessed 16 May 2023).
46. **Tsao YF, Hsu HT and Desai A** (2023) High power handling GaAs SP4T Switch-based Beam-Switching planar antenna module for 5G New-Radio FR2 applications. *AEU - International Journal of Electronics and Communications* **159**(154494), 154494.

Dr. Balaka Biswas received her B.E. degree in Electronics and Communication Engineering from the University of Burdwan, West Bengal, and thereafter finished her masters in the year 2008. She received first class first position (gold medal) in M.Tech and subsequently joined in the Ph.D. program in Jadavpur University, Kolkata, with DST-INSPIRE fellowship. She completed her doctorate degree in 2018 in the field of design and development of various ultra-wideband (UWB) antenna using fractal geometries. Currently, she is working in CSIO-CSIR, Chandigarh, as a Senior Research Associate under Scientist Pool scheme, and she is working in Chandigarh University as an Associate Professor at ECE dept. Her recent research is the development of electrically small antenna for biomedical application. She has more than 30 publications in reputed referred journals and conferences. She has also authored one technical book named "Digital Electronics (ISBN: *9788182474482*)." She serves as a reviewer in several top tier journals, like IEEE Trans. on Antenna propagation, IEEE Access, IETE Journals, PIER-C, PIER-M, JEMWA, etc. She is a fellow of IETE, life member of ISSE and Indian Science Congress Association.

https://doi.org/10.1017/S1759078724000400 Published online by Cambridge University Press

Ayan Karmakar received his M.Tech (Electronics & Telecom Engineering) degree from NIT-Durgapur. Currently, he is working in SCL, Chandigarh, as a Scientist-SE. His research interests include design and development of various passive microwave integrated circuits and antennae using silicon-based MIC, RFMEMS, and THz-technology. He has authored one technical book named "Si-RF Technology" (Springer-2019) and co-authored another book titled "Printed Antennas for Future Generation Wireless Communication and Healthcare" (*CRC Publication (2023)*). He has more than 40 publications in refereed journals and conferences. He serves as a reviewer in top tier international journals, like IEEE Access, RF-MiCAE, Springer, EJAET, etc. He is the fellow of IETE and life member of Indian Science Congress Association and ISSE.

https://doi.org/10.1017/S1759078724000400 Published online by Cambridge University Press